NeuroImage xxx (2011) xxx–xxx

Contents lists available at ScienceDirect

NeuroImage

journal homepage: www.elsevier.com/locate/ynimg

Super-resolution track-density imaging studies of mouse brain: Comparison to histology

Fernando Calamante [a,b,*], Jacques-Donald Tournier [a,b], Nyoman D. Kurniawan [c], Zhengyi Yang [c], Erika Gyengesi [d], Graham J. Galloway [c], David C. Reutens [c], Alan Connelly [a,b]

[a] Brain Research Institute, Florey Neuroscience Institutes, Heidelberg, Victoria, Australia
[b] Department of Medicine, Austin Health and Northern Health, University of Melbourne, Melbourne, Victoria, Australia
[c] Centre for Advanced Imaging, The University of Queensland, Brisbane, Queensland, Australia
[d] Neuroscience Research Australia, Randwick, New South Wales, Australia

ARTICLE INFO

Article history:
Received 14 April 2011
Revised 10 June 2011
Accepted 5 July 2011
Available online xxxx

Keywords:
Magnetic resonance imaging
Super-resolution
Mouse brain
Diffusion MRI
Validation
Histology

ABSTRACT

The recently proposed track-density imaging (TDI) technique was introduced as a means to achieve super-resolution using diffusion MRI. This technique is able to increase the spatial resolution of the reconstructed images beyond the acquired MRI resolution by incorporating information from whole-brain fibre-tracking results. It not only achieves super-resolution, but also provides very high anatomical contrast with a new MRI contrast mechanism. However, the anatomical information-content of this novel contrast mechanism has not yet been assessed. In this work, we perform such a study using diffusion MRI of ex vivo mouse brains acquired at 16.4T, to compare the results of the super-resolution TDI technique with histological staining (myelin and Nissl stains) in the same brains. Furthermore, a modified version of the directionally-encoded colour TDI map using short-tracks is introduced, which reduces the TDI intensity dynamic range, and therefore enhances the directionality colour-contrast. Good agreement was observed between structures visualised in the super-resolution TDI maps and in the histological sections, supporting the anatomical information-content of the images generated using the TDI technique. The results therefore show that the TDI methodology does provide meaningful and rich anatomical contrast, in addition to achieving super-resolution. Furthermore, this study is the first to show the application of TDI to mouse brain imaging: the high-resolution, high-quality images demonstrate the useful complementary information that can be achieved using super-resolution TDI.

Introduction

A new method to achieve super-resolution using diffusion MRI has been recently introduced (Calamante et al., 2010). This technique, referred to as super-resolution track-density imaging (TDI), is able to increase the spatial resolution of the reconstructed images beyond the acquired MRI resolution by incorporating information contained in whole-brain fibre-tracking results. For example, from 2.5 million tracks obtained using probabilistic fibre-tracking, human brain TDI maps with 125 μm isotropic resolution were created from diffusion MRI data acquired with 2.3 mm resolution on a 3 Tesla standard clinical scanner (Calamante et al., 2010), i.e. an approximately 6000-fold reduction in the voxel size. More recently, the super-resolution property of the TDI method was validated (Calamante et al., 2011), using both in vivo high-resolution human diffusion MRI data acquired at 7 T, and in silico diffusion MRI data from a well-characterised numerical phantom (Close et al., 2009). In that study, it was shown that the structures that could be identified in the TDI maps only after using super-resolution were consistent with the corresponding structures identified in the reference high-resolution maps without super-resolution (Calamante et al., 2011).

Abbreviations: 2D, two-dimensional; 3D, three-dimensional; aca, anterior commissure, anterior part; acp, anterior commissure, posterior part; Br, Bregma; cc, corpus callosum; cg, cingulum; cp, cerebral peduncle; CPu, caudate putamen (striatum); CSD, constrained spherical deconvolution; DEC, directionally-encoded colour; δ, duration of the diffusion-weighted gradient pulse; Δ, time-interval between the onset of the two gradient pulses; dhc, dorsal hippocampal commissure; ec, external capsule; eml, external medullary lamina; f, fornix; FA, fractional anisotropy; fi, fimbria of the hippocampus; fmi, forceps minor of the corpus callosum; FOD, fibre orientation distributions; fr, fasciculus retroflexus; gcc, genu of the corpus callosum; Hb, habenula; ic, internal capsule; iFOD2, 2nd order integration over fibre orientation distributions; IMD, intermediodorsal thalamic nucleus; *lmax*, maximum harmonic order; LMol, stratum lacunosum-moleculare; lo, lateral olfactory tract; mfb, medial forebrain bundle; ml, medial lemniscus; MS, medial septal nucleus; mt, mammillothalamic tract; ns, nigrostriatal tract; opt, optic tract; PB, phosphate buffer; pf, precommissural fornix; RGB, red–green–blue; sm, stria medullaris; st, stria terminalis; str, superior thalamic radiation; *st*TDI, short-tracks track density imaging; tc, thalamic commissure; TDI, track density imaging; TE, echo-time; TR, repetition-time.

* Corresponding author at: Brain Research Institute, Florey Neuroscience Institutes, Melbourne Brain Centre, 245 Burgundy Street, Heidelberg, Victoria 3084, Australia. Fax: +61 3 9035 7307.
E-mail address: fercala@brain.org.au (F. Calamante).

1053-8119/$ – see front matter © 2011 Elsevier Inc. All rights reserved.
doi:10.1016/j.neuroimage.2011.07.014

The TDI technique not only provides a means to achieve super-resolution, but it also provides very high anatomical contrast, with a new MRI contrast mechanism not available from other MRI modalities (Calamante et al., 2010). However, the *anatomical information-content* of this novel contrast mechanism has not yet been thoroughly assessed. It remains to be shown whether the features identified on TDI maps correspond to real brain structures, which requires comparison of the TDI maps with an *anatomical* "gold-standard"; while no perfect version of the latter is available, it is widely accepted that histological staining of brain sections provides a very good representation of many structures.

This study attempts to fill this gap by investigating the anatomical information-content of the TDI technique. Diffusion MRI of ex vivo mouse brains was acquired at ultra-high magnetic field strength (16.4 T), and the results of the super-resolution TDI technique were compared to histological staining of the same brains, using Gallyas silver stain for myelin and Nissl stain for cell bodies. Anatomical features were identified in the super-resolution TDI maps, and their appearance and location were visually compared to features in the histological images.

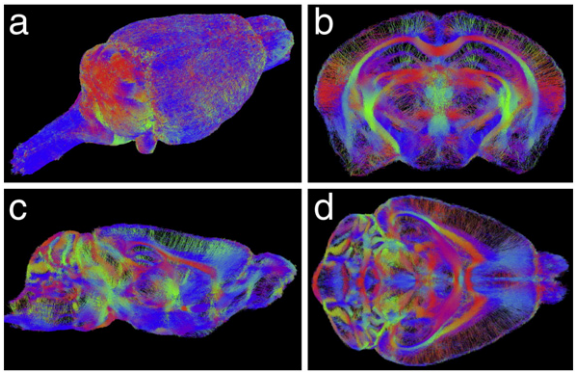

Fig. 1. Example of whole-brain fibre-tracking results from mouse *m3*. (a) Surface view from a dorso-posterior direction. (b) Coronal section, (c) sagittal section, and (d) horizontal section of whole-brain fibre-tracking results; each section displays the tracks within a 0.2 mm slab. The colour-coding indicates the local fibre orientation (red: left–right, green: dorsal–ventral, blue: cranial–caudal). The results correspond to 100,000 tracks. (For interpretation of the references to colour in this figure legend, the reader is referred to the web version of this article.)

Materials and methods

Three 12-week old adult C57 BL6 mice (*m1*, *m2* and *m3*) were included in this study. Mice were anaesthetised and perfused with 4% paraformaldehyde containing 0.5% Magnevist. The brains were removed from the skull and placed in Fomblin for MRI. All mice were housed and handled in accordance with Queensland Animal Care and Protection Act 2001 and the current NHMRC Australian Code of Practice for the Care and Use of Animals for Scientific Purposes (UQ ethics approval CMR/907/08/NHMRC).

MRI data acquisition

Diffusion MRI data were acquired using previously published protocols (Moldrich et al., 2010). In brief, MRI data were acquired on a 16.4 Tesla vertical bore animal system (Bruker Biospin, Germany) using Micro2.5 gradient system and a 15 mm linear surface coil (M2M, Australia). The diffusion acquisition consisted of a 3D diffusion-weighted spin-echo sequence, with TE/TR = 22.8/400 ms, 0.1 mm isotropic resolution, field-of-view: $11.2 \times 19 \times 8$ mm (for mouse *m1* and *m2*) or $11.5 \times 22 \times 8.5$ mm (for mouse *m3*), two $b = 0$ s/mm^2 images and 30 uniformly distributed diffusion gradient-encoding directions (Jones et al., 1999) with $b = 5000$ s/mm^2 ($\delta/\Delta = 2.5/14$ ms). Data acquisition was performed at 22°, with a total acquisition time of ~32 h.

Fibre-tracking

Mouse whole-brain fibre-tracking was carried out using in-house software based on *MRtrix* (Brain Research Institute, Melbourne, Australia, http://www.brain.org.au/software/). The analysis included constrained spherical deconvolution (CSD) (Tournier et al., 2007) to model multiple fibre orientations in each voxel, with a maximum harmonic order $l_{max} = 6$; this parameter determines the 'sharpness' of the fibre orientation distributions (Tournier et al., 2004, 2008). Probabilistic fibre-tracking (Behrens et al., 2003) was performed using the 2nd order integration over fibre orientation distributions (iFOD2) algorithm (Tournier et al., 2010); this included the following relevant parameters: 0.1 mm step-size, maximum angle between steps = 45°, three FOD samples/step, any track with length <0.4 mm was discarded, termination criteria: exit the brain or when the CSD fibre-orientation distribution amplitude was <0.01 (Note: this FOD cut-off value was reduced compared with that used for in vivo human brain studies (Calamante et al., 2011; Tournier et al., 2010), and was empirically chosen based on a preliminary visual assessment of the fibre-tracking results from one of the ex vivo mouse brains; the histological data were not used during this empirical tuning). To achieve whole-brain tracking, random seeds were placed throughout the mouse brain, and tracking was performed bi-directionally. A total of 4,000,000 tracks were generated for each mouse data-set.

Track-density imaging (TDI)

TDI maps were generated using *MRtrix* by calculating the total number of tracks present in each element of a grid. By selecting a grid-element smaller than the voxel size of the source data, the spatial resolution of the final map can be increased, thus achieving super-resolution (see Calamante et al. (2010) for further details). For each mouse dataset, a 20 μm isotropic grid was used to generate the super-

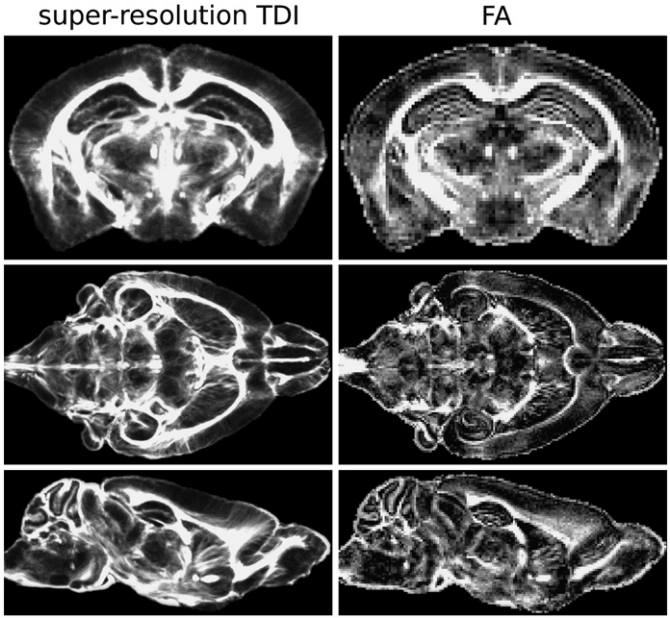

Fig. 2. Super-resolution TDI maps (left column) and FA maps (right column), for coronal (top), horizontal (middle) and sagittal (bottom) orientations. The TDI maps have 20 μm isotropic resolution; the FA maps have 100 μm resolution (i.e. the resolution of the acquired diffusion-weighted imaging data). The data correspond to mouse *m3*.

Please cite this article as: Calamante, F., et al., Super-resolution track-density imaging studies of mouse brain: Comparison to histology, NeuroImage (2011), doi:10.1016/j.neuroimage.2011.07.014

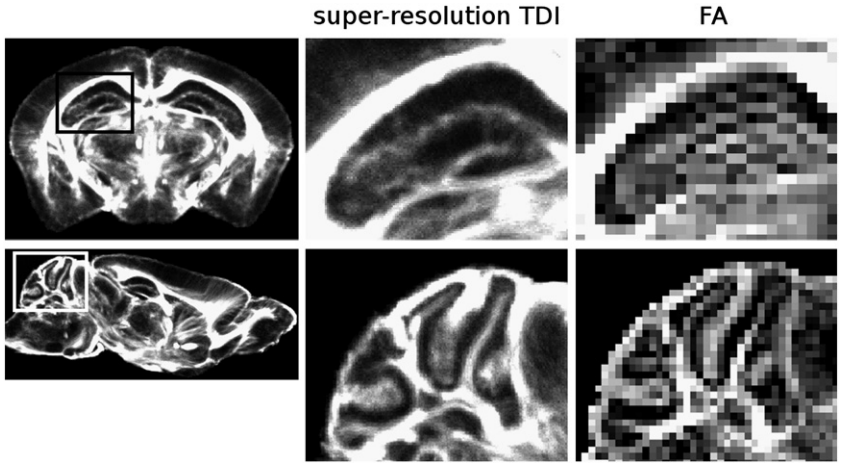

Fig. 3. Zoomed regions of super-resolution TDI maps (middle column) and FA maps (right column). The zoomed region is indicated by the rectangle on the TDI maps shown in the left column. Top row: coronal slice with zoomed region in the hippocampus; bottom row: sagittal slice with zoomed region in the cerebellum. The TDI maps have 20 μm isotropic resolution; the FA maps have 100 μm resolution. The data correspond to mouse *m3*.

resolution TDI map; this corresponds to a 125-fold reduction in the voxel size compared to the acquired resolution.

Modified directionally-encoded colour (DEC) TDI

A directionally-encoded colour (DEC) version of the TDI maps was proposed previously (Calamante et al., 2010) as the super-resolution equivalent of the conventional DEC map in diffusion tensor imaging. One limitation of these super-resolution DEC maps is that the increased dynamic range of the TDI map (as compared with that of the fractional anisotropy map used in the diffusion tensor case (Pajevic and Pierpaoli, 1999)) compromises the visual appearance of low-intensity structures in the TDI map. This is particularly the case in the mouse brain, where the major white matter structures (e.g. the corpus callosum) have a much larger signal intensity in the TDI map (e.g. see Fig. 2). To overcome this limitation, a modified version of the DEC TDI maps was created by *constraining* the maximum length of each track to 1 mm (NB. since this length corresponds to 10 acquired voxels, sufficient medium-range fibre-tracking information is retained to allow the super-resolution step to introduce meaningful intra-voxel information). The resulting DEC TDI map will be referred to as *DEC short-tracks TDI (stTDI)* map. By constraining the length of the tracks, the contribution of each seed-point within a long white matter bundle (e.g. corpus callosum) only contributes to the TDI values within a 1 mm neighbourhood, thus reducing the TDI contrast. Importantly, this improves the visual appearance of the colour-

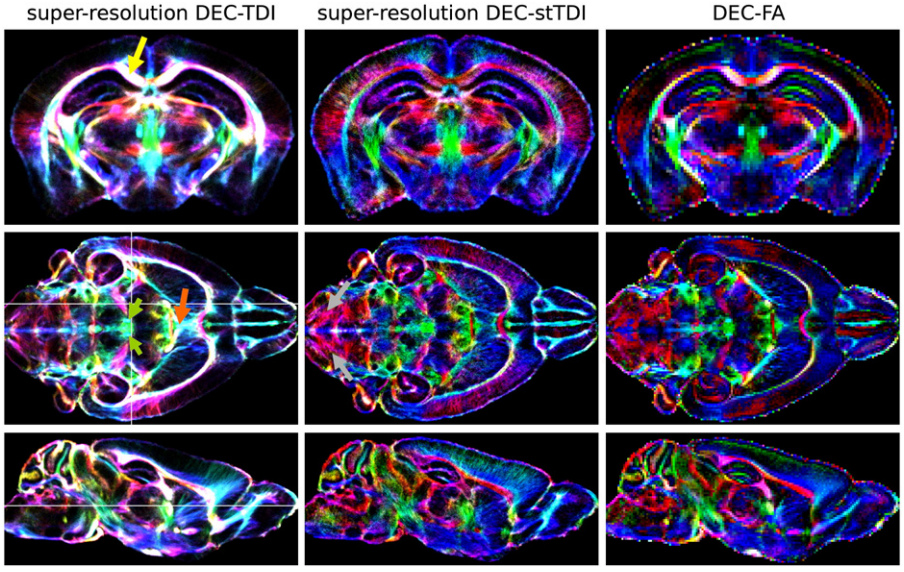

Fig. 4. Directionally-encoded colour (DEC) TDI maps (left column), DEC *st*TDI maps (middle column), and conventional tensor-based DEC maps (right column), for coronal (top), horizontal (middle) and sagittal (bottom) orientations (note: these slices correspond to the same slices displayed in Fig. 2, whose anatomical locations are indicated by the white lines in the first column of Fig. 4). The colour-coding indicates the local fibre orientation (for the TDI maps) or the principal direction of the diffusion tensor (for the tensor-based map). Red: left–right, green: dorsal–ventral, blue: rostral–caudal. The TDI-based DEC maps have 20 μm isotropic resolution; the tensor based DEC maps have 100 μm resolution. The DEC *st*TDI maps display good directionality information in both long and short bundles (e.g. see yellow, green, orange, and grey arrows for the corpus callosum, the fasciculus retroflexus, the fornix precommissuralis, and the solitary tract, respectively); some of these structures have very high intensity (and therefore appear 'saturated') in the DEC-TDI maps, or they have very low intensity and are barely seen in these maps. The data correspond to mouse *m3*. (For interpretation of the references to colour in this figure legend, the reader is referred to the web version of this article.)

Please cite this article as: Calamante, F., et al., Super-resolution track-density imaging studies of mouse brain: Comparison to histology, NeuroImage (2011), doi:10.1016/j.neuroimage.2011.07.014

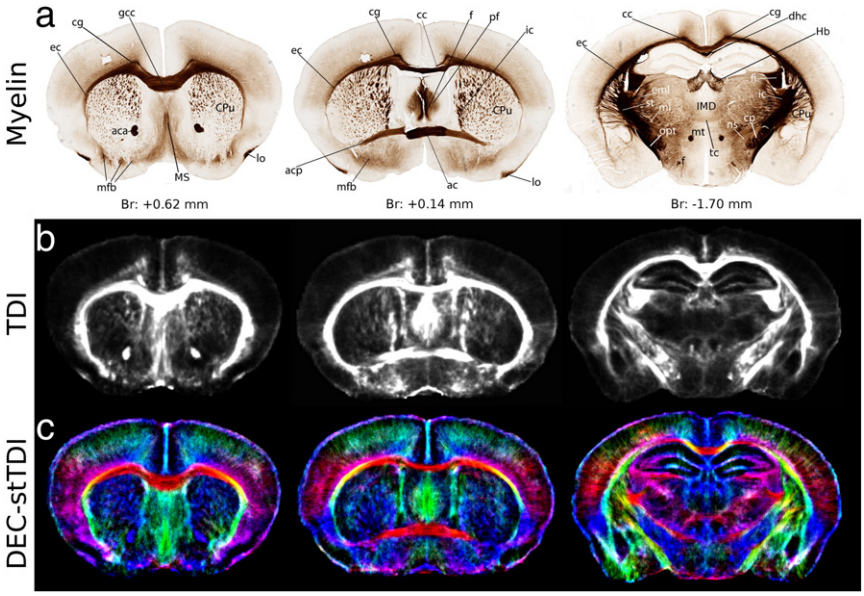

Fig. 5. Comparison of TDI maps with myelin staining for the brain of mouse *m1*. Example coronal slices (at three different anatomical positions) from: (a) myelin staining, (b) super-resolution TDI maps, and (c) super-resolution DEC *st*TDI maps. The colour-coding indicate the local fibre orientation (red: left–right, green: dorsal–ventral, blue: rostral–caudal). The super-resolution maps have 20 μm isotropic resolution. The distance to Bregma for each histological slice is indicated in the figure. Abbreviations: aca — anterior commissure, anterior part; acp — anterior commissure, posterior part; cc — corpus callosum; cg — cingulum; cp — cerebral peduncle; CPu — Caudate putamen (striatum); dhc — dorsal hippocampal commisure; ec — external capsule; eml — external medullary lamina; f — fornix; fi — fimbria of the hippocampus; fmi — forceps minor of the corpus callosum; fr — fasciculus retroflexus; gcc — genu of the corpus callosum; Hb — habenula; IMD — intermediodorsal thalamic nucleus; ic — internal capsule; lo — lateral olfactory tract; mfb — medial forebrain bundle; ml — medial lemniscus; MS — medial septal nucleus; mt — mammillothalamic tract; ns — nigrostriatal tract; opt — optic tract; pf — precommissural fornix; sm — stria medullaris; st — stria terminalis; str — superior thalamic radiation; tc — thalamic commissure.

contrast in the DEC *st*TDI maps (note that in the DEC maps the relevant contrast information is contained in the colour, rather than the image intensity). However, since the TDI intensity is greatly reduced overall (each shorter track only contributes intensity to a smaller number of voxels), a much larger number of tracks need to be generated to maintain a reasonable contrast-to-noise ratio. For this study, 65 million tracks were therefore generated for each mouse brain data-set with the short track constraint, and DEC *st*TDI maps constructed with 20 μm isotropic resolution.

Histology

Histology was performed with myelin staining for the brains of mice *m1* and *m2,* and Nissl staining (cell bodies) for mouse *m3*. For myelin staining, animals were anaesthetized and transcardially perfused with saline followed by ice-cold 4% paraformaldehyde in 0.1 M phosphate buffer (PB) (pH = 7.4). The brains were removed and immersed in 30% sucrose in 0.1 M PB for cryoprotection for 12 h. The next day, 40 μm coronal sections of the entire brains were cut by using a cryostat (Leica, Germany), and placed in 10% formalin for 3–5 days for myelin staining. Myelin staining first described by Gallyas (Gallyas, 1971, 1979) was carried out on free-floating sections as modified by Pistorio et al. (2006). Briefly, after pre-treatment with a lipid solvent (2:1 pyridine: acetic anhydride) for 30 min, sections were rehydrated in washes of decreasing concentrated pyridine, then immersed into colloidal silver nitrate solution for impregnation. In the next step, the sections were placed back into 10% formalin. After the developing of the silver particles in the developer solution, sections were immersed into the bleaching solution for de-staining, in cases when it was necessary (Pistorio et al., 2006). After the myelin staining procedure, the sections were mounted on gelatine coated slides and cover slipped after dehydration with DePex (Electron Microscopy Sciences, USA). Slides were scanned with a ScanScope XT (Aperio, USA) bright field scanner at 20× magnification and digital images edited with Adobe Photoshop CS4.

For Nissl staining, the perfusion fixed brain was immersed in 30% sucrose solution in 0.1 M PB (pH = 7.4). Tissue was then embedded in a mould containing 5% gelatin in 0.1 M PB and frozen in an isopentane bath cooled in liquid nitrogen. Coronal serial sections (40 μm) were cut using a Leica sliding microtome. The slides were prepared by washing with ethanol and xylene, and subsequently rehydrated prior to staining using 0.1% Cresyl Violet for 5 min. These slides were then washed using ethanol and xylene and mounted in DePex medium.

Image registration

For the *m1* and *m2* mice, the TDI slices closest to the available histological sections were visually identified. For the *m3* mouse, since a sufficient number of histological sections were available, these were reconstructed as a 3D stack and registered to the TDI maps. A dedicated iterative registration method was used to reconstruct the histological volume by stacking the histological sections with the guidance of a structural MRI volume. Structural MRI was employed not only for the correction of the overall shape of histological volume, but also to deal with the split parts problem of histological sections. The method was initialized by aligning adjacent 2D histological sections using a local rigid registration method to form an estimation of the 3D volume, to which the structural MRI volume was co-registered using a 9-parameter affine registration method to find the corresponding MRI slice for each histological section. Histological sections were then registered to the corresponding MRI slices to create an updated 3D volume, and the structural MRI was aligned to it again. This procedure was repeated until there was no significant improvement observed in terms of 3D registration quality. The reconstructed histological volume was then affine registered and non-linearly warped onto the original structural MRI volume. TDI

Please cite this article as: Calamante, F., et al., Super-resolution track-density imaging studies of mouse brain: Comparison to histology, NeuroImage (2011), doi:10.1016/j.neuroimage.2011.07.014

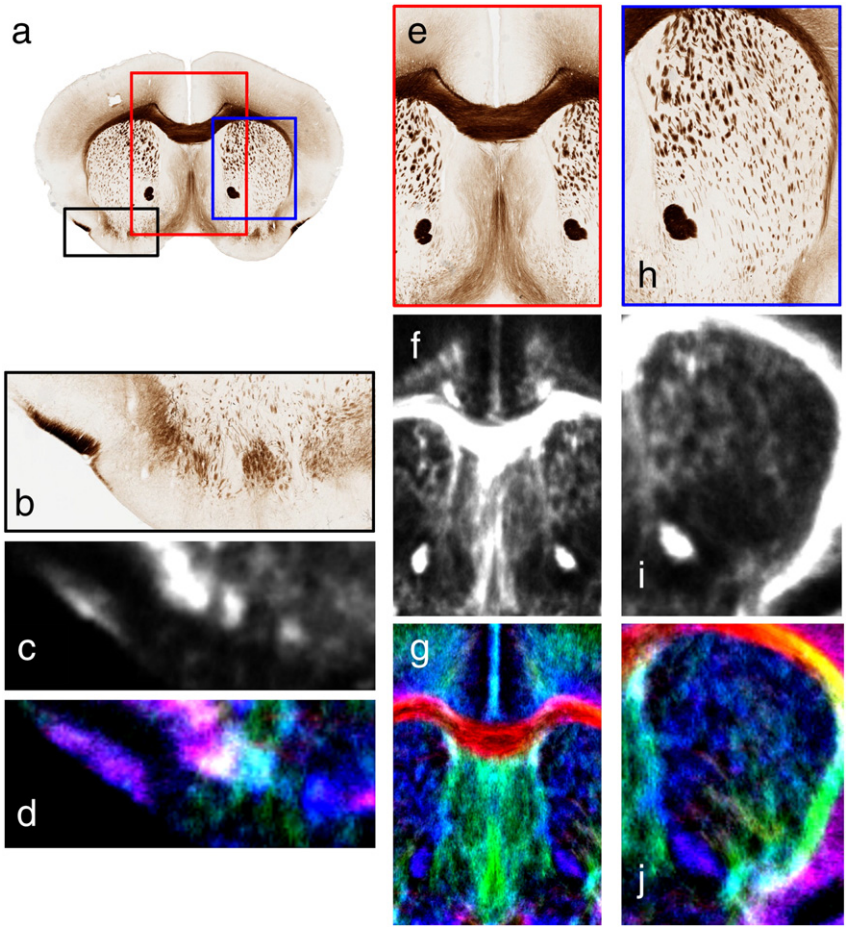

Fig. 6. Zoomed regions of the coronal slice shown in left column of Fig. 5. Each column shows the myelin staining, super-resolution TDI maps and super-resolution DEC *st*TDI maps, with the zoomed areas indicated by the black (left column), red (middle column), and blue (right column) boxes in Fig. 6a. The colour-coding in figures d, g, and j indicates the local fibre orientation (red: left–right, green: dorsal–ventral, blue: rostral–caudal). The super-resolution maps have 20 μm isotropic resolution. (For interpretation of the references to colour in this figure legend, the reader is referred to the web version of this article.)

maps of the same brain were rigidly aligned to the original structural MRI volume. This processing pipeline resulted in a co-registered TDI maps and histological volumes in the same reference space as the structural MRI volume.

Results

High quality and high-resolution diffusion MRI data were obtained with our protocol; as reference, the signal-to-noise ratio of the $b = 0$ s/mm^2 image was ~55. Fig. 1 shows representative examples of whole-brain fibre-tracking results in the mouse brain. For visualisation purposes, only 100,000 tracks have been displayed. As can be appreciated in the figure, the combination of CSD and iFOD2 tracking produce very high-quality whole-brain fibre-tracking results from these diffusion MRI data.

Fig. 2 shows a typical example of coronal, horizontal and sagittal TDI maps, as well as the corresponding native-resolution fractional anisotropy (FA) maps. The FA maps have been included to illustrate the increase in spatial resolution achieved by super-resolution, as well as to emphasise the different contrast information present in the TDI maps. The increase in spatial resolution can be further appreciated in the zoomed examples displayed in Fig. 3, where the sharper delineation of the complex structures in the hippocampus and cerebellum is clearly visible in the super-resolution TDI maps.

Regions of TDI hyperintensity also can be seen in somewhat unexpected areas; for example, in the superior midline (top-left image in Fig. 2) and the exterior layer of the brain and cerebellum (bottom-left image in Fig. 2). These bright areas on TDI are also high on the equivalent FA maps (images in the right column in Fig. 2), indicating the presence of diffusion anisotropy in these areas. The source of this anisotropy is likely to be related to the meninges, including the pia mater and arachnoid mater. This layer is visible in our diffusion MRI images due to its relatively organised structure, and the high spatial-resolution and SNR of the acquired images.

Fig. 4 shows the corresponding DEC TDI maps (first column), DEC *st*TDI maps (second column) and conventional tensor-based DEC maps (third column), with the RGB colour-coding indicating the average local orientation. These images illustrate the increased directional information in the DEC *st*TDI maps (cf. DEC TDI maps). Due to their track-length constraint, the DEC *st*TDI maps display good directional information in both long tracts (such as the corpus callosum, the fasciculus retroflexus and the fornix precommissuralis: see yellow, green and orange arrows respectively), short bundles (such as the solitary tract, see grey arrows), and in cortical areas. Furthermore, the DEC *st*TDI maps still retain the super-resolution properties of the TDI method, thus showing increased resolution compared to the conventional DEC maps. Despite the increase in resolution in the DEC-TDI maps, there are some structures that are still more conspicuous in the DEC-FA maps; for example, the thin green band (corresponding to dorsal–ventral orientation) near the surface of the cortex in the coronal map (top-right image in Fig. 4), or some interior portions of the hippocampus (e.g. green thin bands on

Please cite this article as: Calamante, F., et al., Super-resolution track-density imaging studies of mouse brain: Comparison to histology, NeuroImage (2011), doi:10.1016/j.neuroimage.2011.07.014

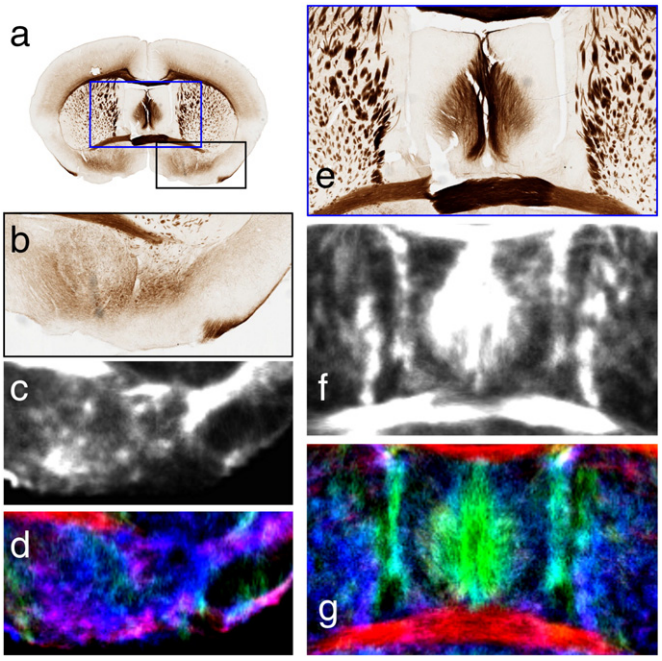

Fig. 7. Zoomed regions of the coronal slice shown in middle column of Fig. 5. Each column shows the myelin staining, super-resolution TDI maps and super-resolution DEC *st*TDI maps, with the zoomed areas indicated by the black (left column) and blue (right column) boxes in Fig. 7a. The colour-coding in figures d and g indicates the local fibre orientation (red: left–right, green: dorsal–ventral, blue: rostral–caudal). The super-resolution maps have 20 μm isotropic resolution. (For interpretation of the references to colour in this figure legend, the reader is referred to the web version of this article.)

the coronal view). These structures are present in the DEC-TDI maps, but they are much less apparent; these short structures have less relative intensity in the TDI maps (even when using the *st*TDI version).

A comparison of the structures visualised in the TDI maps and those identified in myelin staining in the *m1* mouse is shown in Fig. 5 for a representative subset of coronal slices. As can be appreciated in these images, there is a striking correspondence between many of the structures present in both imaging modalities. These include major white matter tracts (such as the corpus callosum, anterior commissure, internal and external capsules, cerebral peduncle, optic tract, etc.), smaller white matter structures (such as cingulum, medial forebrain bundle, lateral olfactory tract, mammillothalamic tract, fornix, precommissural fornix, etc.), the hippocampus and several structures around the deep grey matter (e.g. see complex shape of hippocampal structures, fimbria of the hippocampus nigrostriatal tract, medial lemniscus, and even the 'texture' in the striatum area), as well as cortical areas.

To further highlight the correspondence between the TDI maps and myelin histology, Figs. 6–8 show a number of zoomed regions from the 3 coronal slices included in Fig. 5. In particular, Fig. 6 shows zoomed areas of the same anatomical location as that shown in the left column of Fig. 5, highlighting: (b–d) the medial forebrain bundle and lateral olfactory tract area, (e–g) the genu of the corpus callosum, medial septal nucleus, and anterior part of the anterior commissure area, and (h–j) the external capsule and striatum area (note that the TDI method not only reproduces the 'texture' in the striatum, but also the region with denser TDI hyperintensity structures (i.e. dorsomedial part of the striatum) is consistent with the region with denser features in the myelin staining); see Fig. 5 for a detailed list and locations of the various anatomical structures.

Similarly, Fig. 7 shows zoomed regions from the middle column of Fig. 5, highlighting: the medial forebrain bundle and lateral olfactory tract area (b–d), and the anterior commissure, corpus callosum, cingulum, internal capsule, fornix and precommissural fornix area (e–g).

Fig. 8 shows equivalent zoomed regions from the right column of Fig. 5, highlighting: the hippocampus, fimbria of the hippocampus, dorsal hippocampal commissure, corpus callosum, and cingulum, area (b–d), the mammillothalamic tract, habenula, intermediodorsal thalamic nucleus, and thalamic commissure area (e–g), and the cerebral peduncle, striatum, internal and external capsules, fornix, medial lemniscus, nigrostriatal tract, optic tract, and fimbria of the hippocampus area (h–j).

It should be noted, however, that there are also a number of anatomical features in the TDI maps (particularly on the DEC-*st*TDI maps, which contain increased anatomical information given by the local orientation of the structures), which do not have an obvious correlate in the histological images (see the Discussion section for more details).

Fig. 9 shows equivalent results for the data from the *m2* mouse. In this case, a larger number of coronal slices have been displayed to enable a visual comparison between the TDI maps and myelin staining images over a larger extent, from rostral to caudal slices including the cerebellum. Once again, the visual correspondence between many of the structures across the various coronal levels can be clearly appreciated, from the major white matter tracts, to smaller white matter structures, sub-cortical structures, as well as the convoluted structures of the cerebellum.

Fig. 10 shows an equivalent comparison for the *m3* mouse, with the corresponding TDI maps and Nissl staining images shown for a representative subset of horizontal slices. Once again, the similarity between many of the structures visualised by both imaging modalities is readily appreciated. These include not only the major white matter tracts, but also a number of other brain features; for example, the change in shape of the complex hippocampus structures in the various horizontal slices is well-represented in the TDI maps. Similarly, the convoluted cerebellum sulci are reconstructed by the TDI technique with great detail, including the very small sulci (see also zoomed image in the right column of Fig. 11 for greater detail).

To highlight some further examples, Fig. 11 also shows other zoomed areas from the horizontal sections. These images show that TDI reconstructs not only the major structures (e.g. the corpus callosum, external capsule, fornix), but also some other structures such as the fornix, fasciculus retroflexus, internal capsule and superior thalamic radiation area (left column in Fig. 11), and even the 'texture' of the structures in the striatum area (middle column in Fig. 11). Note that the striped appearance of the Nissl stained images is due to the 3D reconstruction process (the images were acquired in coronal orientation). Fig. 12 shows two coronal slices of the same dataset, with zoomed regions highlighting the hippocampus and surrounding area (left column) and the fasciculus retroflexus, medial lemniscus, mammillothalamic tract, and external medullary lamina area (right column). There is clear agreement between many of the structures observed using both modalities, including those above.

Discussion

We have presented an assessment of the anatomical information-content of the TDI technique by comparing the structures visualised in TDI maps from mouse brains with those identified in histological staining of the same brains. The striking agreement between structures visualised in the super-resolution TDI maps and the myelin and Nissl stained histological sections corroborates the anatomical information-content of the images generated using the TDI technique. The results therefore show that the TDI methodology provides a rich anatomical contrast that is biologically meaningful. The current study

Please cite this article as: Calamante, F., et al., Super-resolution track-density imaging studies of mouse brain: Comparison to histology, NeuroImage (2011), doi:10.1016/j.neuroimage.2011.07.014

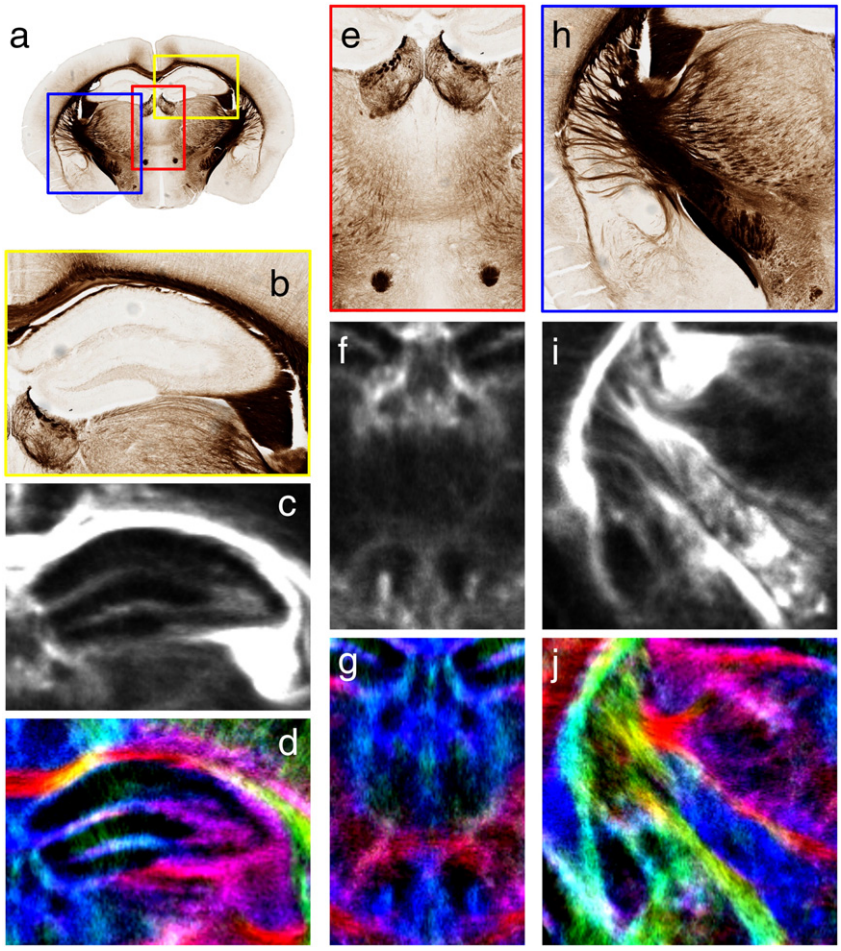

Fig. 8. Zoomed regions of the coronal slice shown in right column of Fig. 5. Each column shows the myelin staining, super-resolution TDI maps and super-resolution DEC *st*TDI maps, with the zoomed areas indicated by the yellow (left column), red (middle column), and blue (right column) boxes in Fig. 8a. The colour-coding in figures d, g, and j indicates the local fibre orientation (red: left–right, green: dorsal–ventral, blue: rostral–caudal). The super-resolution maps have 20 μm isotropic resolution. (For interpretation of the references to colour in this figure legend, the reader is referred to the web version of this article.)

is therefore complementary to our previous validation of the super-resolution property of TDI (Calamante et al., 2011).

It should be noted that, since the diffusion MRI contrast mechanism is not B_0-dependent, the biologically meaningful TDI contrast demonstrated in the current study using ultra-high field 16.4 T MRI should still be valid for the lower magnetic field strengths more commonly used in experimental and clinical studies (provided suitable acquisition protocols and DWI analysis methods are used to enable reliable fibre-tracking results to be obtained). Therefore, the current results also serve to corroborate the anatomical information of the high-contrast structures demonstrated previously by TDI in human studies at 3T (Calamante et al., 2010).

The comparison between the TDI maps and histological staining in this study was performed in a qualitative manner. A formal quantitative comparison of the agreement between these imaging methodologies is not straightforward due to the different contrast mechanisms. It should be noted that, for the same reason, all of the structures identified in the TDI map are not necessarily expected to have an equivalent in the histological stained images, and vice versa. Furthermore, and more importantly, despite the use of image registration between MRI and histology in two of the mice data-sets (*m2* and *m3*), the presence of residual registration errors is unavoidable.

The myelin and Nissl histological staining included in our study, despite their great utility, can only provide a limited degree of reference for the assessment of the anatomical contrast of the TDI maps, and cannot be considered to constitute a true "gold standard" for the TDI technique. Indeed, validation of fibre-tracking is widely acknowledged to be a significant problem; given that the TDI technique is based on whole-brain fibre-tracking, there is currently no true "gold-standard" that can be used. As a result, and as mentioned above, not all the features in the TDI maps are expected to have a correlate on the histological stained images; however, this does not in itself imply the TDI structures are artificial. It is important to note that whole-brain fibre-tracking may identify an area as highly connected (i.e. a large number of streamlines and, therefore, bright appearance on the TDI map) without this necessarily implying that that white matter bundle will have higher myelin content than nearby white matter areas (i.e. different intensity in the myelin staining images). This in turn implies that not all the bright areas in the TDI map must correspond to dark areas in the myelin stained images. The two are images of different white matter characteristics: TDI represents the density of streamlines within the whole-brain tracking model, while the myelin staining indicates the myelin content of the brain structure. Nevertheless, despite the fact that perfect correspondence cannot be expected (given the different basis for the image contrast in each case), the comparison is still important in those areas in which direct correspondence between the two modalities serves to corroborate the TDI contrast as corresponding to real structures in the brain rather than processing artefact.

Please cite this article as: Calamante, F., et al., Super-resolution track-density imaging studies of mouse brain: Comparison to histology, NeuroImage (2011), doi:10.1016/j.neuroimage.2011.07.014

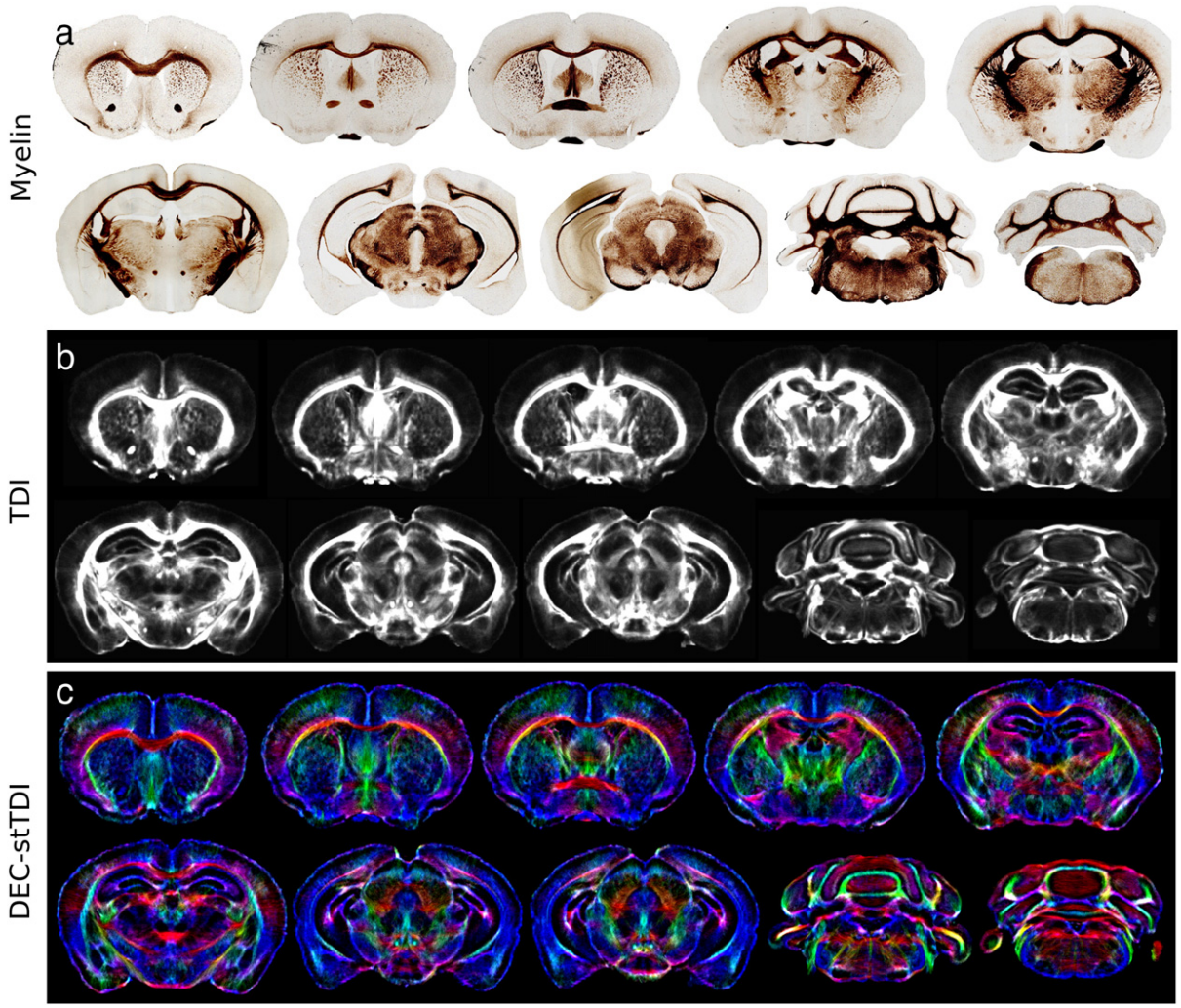

Fig. 9. Comparison of TDI maps with myelin staining for the brain of mouse *m2*. Example coronal slices (at 10 different levels) from myelin staining (a), super-resolution TDI maps (b) and super-resolution DEC *st*TDI maps (c). The colour-coding indicates the local fibre orientation (red: left–right, green: dorsal–ventral, blue: rostral–caudal). The super-resolution maps have 20 μm isotropic resolution. (For interpretation of the references to colour in this figure legend, the reader is referred to the web version of this article.)

A bright structure in a TDI map can only occur where there is a high number of streamlines in the whole-brain fibre-tracking results. Therefore, the *anatomical* accuracy of the TDI map is directly related to the *anatomical* accuracy (as opposed to the connectivity accuracy) of the whole-brain fibre-tracking results. While fibre-tracking is known for its sensitivity to false positives and false negatives, TDI could be considered as one of the 'safest' applications of fibre-tracking. This is mainly for 2 reasons: (*i*) it relies only on *whole-brain* fibre-tracking, thus eliminating a major source of subjectivity in fibre-tracking (namely the definition of seed/target regions); *(ii)* for its anatomical detail, TDI relies only on the streamlines generated by fibre-tracking being spatially in the correct place, and not that any implied connectivity is correct; the latter only affects the relative *intensity* of the TDI image, but not the *location* of the structures in the map (Calamante et al., 2010). In other words, for the anatomical detail in the TDI maps to be correct, it is important that in the location where whole-brain fibre tracking identified a streamline, a coherently oriented brain structure is actually present. This assumption is not unrealistic.

Despite the limitations discussed above, the histological images included in our study nevertheless do provide a good reference for comparison with TDI. As expected, the myelin stain provided more relevant anatomical detail for assessment of a diffusion MRI based method such as TDI; many more white matter features are better visualised in the myelin stained than in the Nissl stained images. However, as could be also appreciated in the human histological sections included in our 2010 article (please see Fig. 2 in Calamante et al., 2010), the borders of many of the structures visualised by the cell staining show reasonably good agreement with those visualised by myelin staining. A similar situation occurs in our mouse brain data, and the borders of many, but not all of the Nissl stained regions can be also used as reference for comparison with our TDI images.

This study also introduces a variant of the DEC TDI technique, the so-called DEC *st*TDI, which reduces the dynamic range of the intensity of the TDI maps while still retaining the directional information. Therefore, the DEC *st*TDI maps retain high local fibre directional contrast (encoded by the RGB colours), while having the benefit of a more uniform intensity than the DEC TDI maps. By constraining the maximum length of each track, the DEC *st*TDI technique does not 'penalise' the DEC contrast in short fibre bundles (cf. DEC TDI maps in Fig. 4). Importantly, since the length constraint is several voxels in length (in our case, 10 acquired voxels), the fibre-tracks still retain medium-range information, and therefore sufficient intra-voxel information to achieve super-resolution. On the other hand, as explained in the Materials and methods section, the number of tracks required to generate the DEC *st*TDI maps is approximately an order of

Please cite this article as: Calamante, F., et al., Super-resolution track-density imaging studies of mouse brain: Comparison to histology, NeuroImage (2011), doi:10.1016/j.neuroimage.2011.07.014

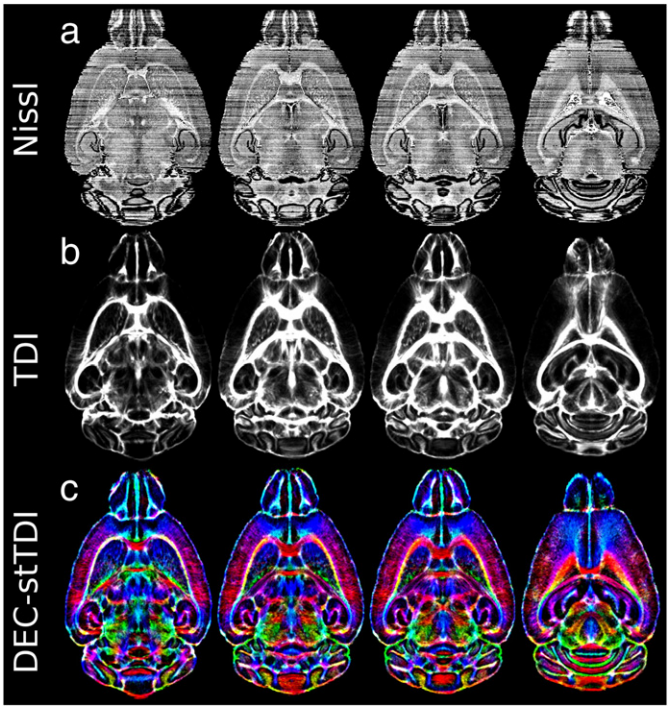

Fig. 10. Comparison of TDI maps with Nissl staining for the brain of mouse *m3*. Example horizontal slices (at four different levels) from: (a) 3D-reconstructed Nissl staining, (b) super-resolution TDI maps, and (c) super-resolution DEC *st*TDI maps. The colour-coding indicates the local fibre orientation (red: left–right, green: dorsal–ventral, blue: rostral–caudal). The super-resolution maps have 20 μm isotropic resolution. (For interpretation of the references to colour in this figure legend, the reader is referred to the web version of this article.)

magnitude greater. However, since each track is much shorter, the processing-time and track file size are similar.

There were some short structures in the DEC maps that were more conspicuous in the DEC-FA maps, such as a thin superficial cortical layer and some internal hippocampal structures (see thin green structures in top-right image in Fig. 4); these short structures have less relative intensity in the TDI maps, thus making them less apparent in the maps. Interestingly, despite the lower conspicuity, the DEC-TDI maps highlight better that these dorsal–ventral oriented structures extend beyond the thin layer displayed by the DEC-FA map (e.g. see cortical area in top-middle image in Fig. 4, and Supplementary Fig. 1); this is consistent with the known limitations of the tensor model (and therefore of the DEC-FA map) to represent areas with multiple fibre orientations; for example, the green region within the cortex corresponds to structures oriented radially to the cortical surface, which traverse other oriented structures in deeper cortical layers, and therefore appear very thin in the DEC-FA maps. Nevertheless, it should be emphasised that the DEC-TDI maps are not intended to replace the DEC-FA maps; analogous to the way that the TDI and FA maps complement each other, the DEC-TDI and DEC-FA maps should also be considered as complementary (since they do not contain the same information, therefore one cannot entirely replace the other).

Apart from evaluating the anatomical information of the TDI methodology, this study is the first to show the application of this new technique to mouse brain imaging. The high-resolution, high-quality images shown in the current study demonstrate the useful complementary information that can be achieved using super-resolution TDI. Due to the increasing interest in mouse brain mapping and imaging phenotypes in mouse models of neurological disorders (e.g. Wadghiri and Helpern, 2007; Waerzeggers et al., 2010), the TDI methodology

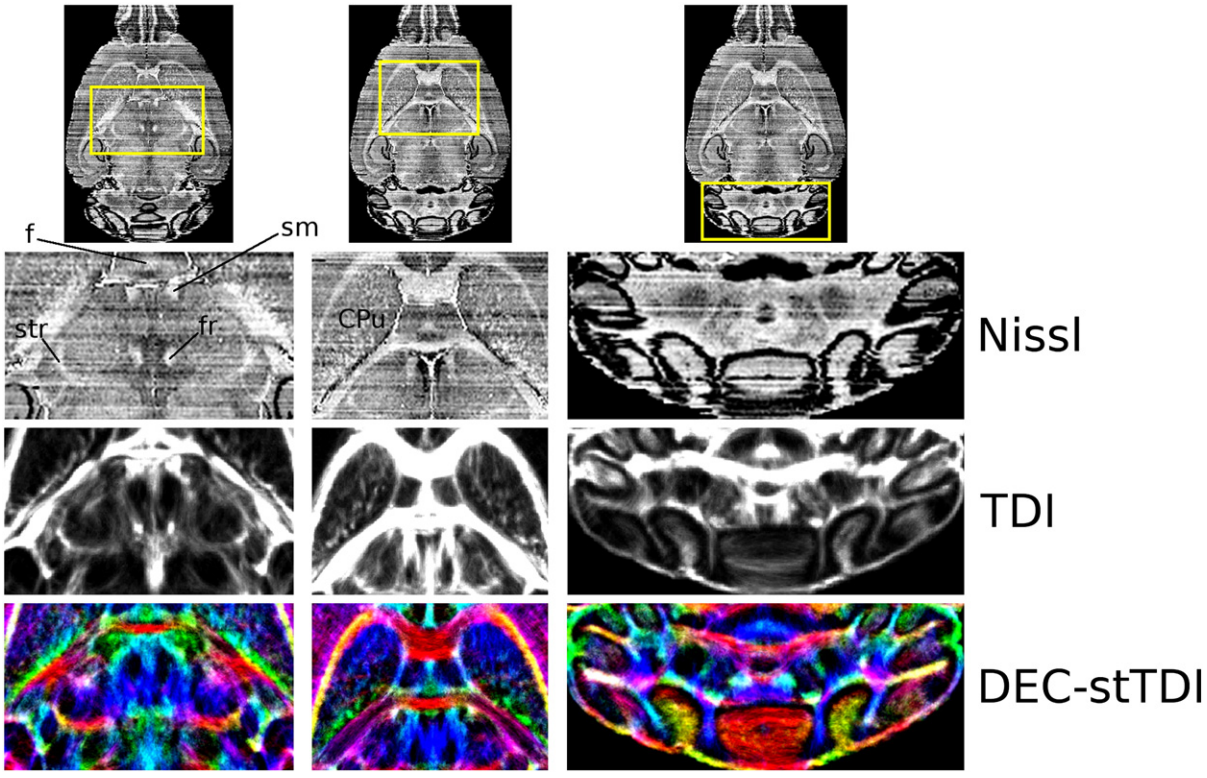

Fig. 11. Zoomed regions of the horizontal slices shown in Fig. 10. The left column corresponds to the same location as that in the first column in Fig. 10; the other two columns correspond to the same location as that in the second column in Fig. 10. Each column shows the Nissl staining, super-resolution TDI maps and super-resolution DEC *st*TDI maps, with the zoomed area indicated by the yellow boxes in the top row. The colour-coding indicates the local fibre orientation (red: left–right, green: dorsal–ventral, blue: rostral–caudal). The super-resolution maps have 20 μm isotropic resolution. Abbreviations: CPu, caudate putamen (striatum); f, fornix; fr, fasciculus retroflexus; sm, stria medullaris; str, superior thalamic radiation. (For interpretation of the references to colour in this figure legend, the reader is referred to the web version of this article.)

Please cite this article as: Calamante, F., et al., Super-resolution track-density imaging studies of mouse brain: Comparison to histology, NeuroImage (2011), doi:10.1016/j.neuroimage.2011.07.014

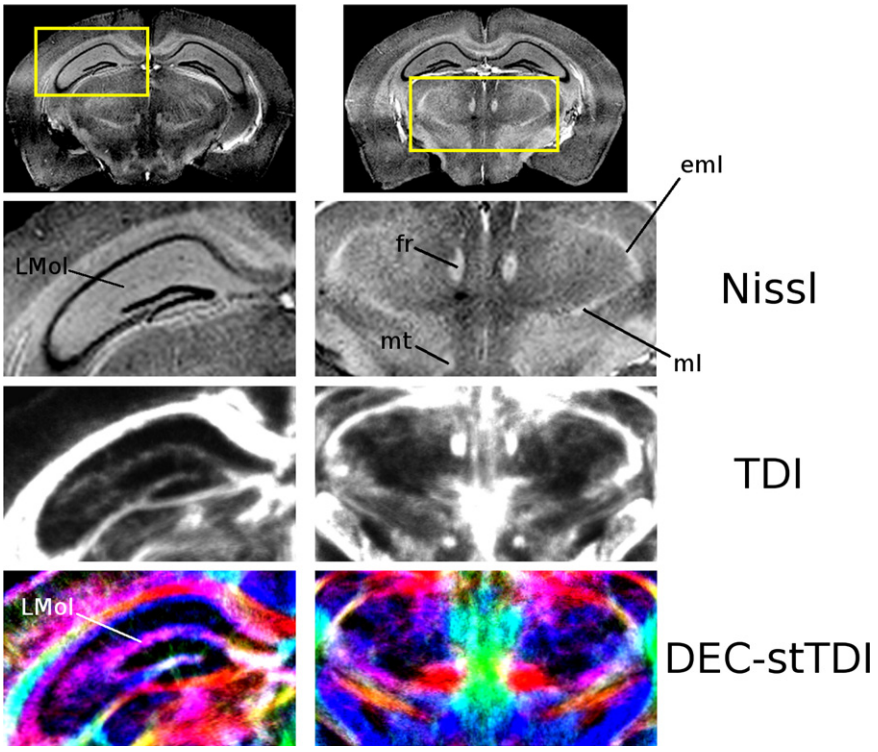

Fig. 12. Comparison of TDI maps with Nissl staining for the brain of mouse *m3*. Example coronal slices (at two different levels). Each column shows the Nissl staining, super-resolution TDI maps and super-resolution DEC *st*TDI maps, with the zoomed area indicated by the yellow boxes in the top row. The colour-coding indicate the local fibre orientation (red: left–right, green: dorsal–ventral, blue: rostral–caudal). The super-resolution maps have 20 μm isotropic resolution. Abbreviations: eml, external medullary lamina; fr, fasciculus retroflexus; LMol, stratum lacunosum-moleculare; ml, medial lemniscus; mt, mammillothalamic tract. (For interpretation of the references to colour in this figure legend, the reader is referred to the web version of this article.)

should provide a very useful additional imaging modality. Furthermore, this methodology could also play an important role in the study of other animal species, when high-resolution imaging with good white matter contrast is needed.

The power of MRI lies in the breadth of available image contrasts, and super-resolution TDI provides one more such modality, which has different properties of very high resolution and novel image contrast (Calamante et al., 2010). It is not the intention of this study to compare TDI with FA maps, or to discuss where TDI provides more information than FA and vice versa. (The usefulness of high-resolution FA and DEC-FA maps to study mouse brain is well-established (e.g. Aggarwal et al., 2010; Chuang et al., 2011; Jiang and Johnson, 2010)). The primary purpose of the present study is to demonstrate that the features seen in the super-resolution TDI maps are largely consistent with features observed in histological sections of the same brains, and are not an artefact of the post-processing steps.

It should be emphasised that the super-resolution property of the TDI approach is not equivalent to interpolation. As shown in our previous studies (e.g. see Fig. 8 in Calamante et al.(2010) and Fig. 4 in Calamante et al. (2011)), interpolation of a map does not provide an equivalent level of resolution to that achieved by the super-resolution TDI method. For example, interpolating a low-resolution TDI map does not produce the same results as a super-resolution TDI map; as expected, interpolation smoothes the image, but the structures delineated remain coarsely defined (Calamante et al., 2010).

In conclusion, the good agreement observed between structures visualised in the super-resolution TDI maps and in the histological sections supports the veracity of the anatomical information-content of the images generated using the TDI technique. Therefore, the TDI methodology does provide rich anatomical information that is biologically meaningful, in addition to achieving super-resolution.

Supplementary materials related to this article can be found online at doi:10.1016/j.neuroimage.2011.07.014.

Acknowledgments

We are grateful to the National Health and Medical Research Council (NHMRC) of Australia, Austin Health, and the Victorian Government's Operational Infrastructure Support Program for their support.

References

Aggarwal, M., Mori, A., Shimogori, T., Blackshaw, S., Zhang, J., 2010. Three-dimensional diffusion tensor microimaging for anatomical characterization of the mouse brain. Magn. Reson. Med. 64, 249–261.

Behrens, T.E., Johansen-Berg, H., Woolrich, M.W., Smith, S.M., Wheeler-Kingshott, C.A., Boulby, P.A., Barker, G.J., Sillery, E.L., Sheehan, K., Ciccarelli, O., Thompson, A.J., Brady, J.M., Matthews, P.M., 2003. Non-invasive mapping of connections between human thalamus and cortex using diffusion imaging. Nat. Neurosci. 6, 750–757.

Calamante, F., Tournier, J.-D., Jackson, G.D., Connelly, A., 2010. Track Density Imaging (TDI): super-resolution white matter imaging using whole-brain track-density mapping. NeuroImage 53, 1233–1243.

Calamante, F., Tournier, J.-D., Heidemann, R.M., Anwander, A., Jackson, G.D., Connelly, A., 2011. Track density imaging (TDI): validation of super-resolution property. NeuroImage 56, 1259–1266.

Chuang, N., Mori, S., Yamamoto, A., Jiang, H., Ye, X., Xu, X., Richards, L.J., Nathans, J., Miller, M.I., Toga, A.W., Sidman, R.L., Zhang, J., 2011. An MRI-based atlas and database of the developing mouse brain. NeuroImage 54, 80–89.

Close, T.G., Tournier, J.-D., Calamante, F., Johnston, L.A., Mareels, I., Connelly, A., 2009. A software tool to generate simulated white matter structures for the assessment of fibre-tracking algorithms. NeuroImage 47, 1288–1300.

Gallyas, F., 1971. A principle for silver staining of tissue elements by physical development. Acta Morphol. Acad. Sci. Hung. 19, 57–71.
Gallyas, F., 1979. Silver staining of myelin by means of physical development. Neurol. Res. 1, 203–209.
Jiang, Y., Johnson, G.A., 2010. Microscopic diffusion tensor imaging of the mouse brain. NeuroImage 50, 465–471.
Jones, D.K., Horsfield, M.A., Simmons, A., 1999. Optimal strategies for measuring diffusion in anisotropic systems by magnetic resonance imaging. Magn. Reson. Med. 42, 515–525.
Moldrich, R.X., Pannek, K., Hoch, R., Rubenstein, J.L., Kurniawan, N.D., Richards, L.J., 2010. Comparative mouse brain tractography of diffusion magnetic resonance imaging. NeuroImage 51, 1027–1036.
Pajevic, S., Pierpaoli, C., 1999. Color schemes to represent the orientation of anisotropic tissues from diffusion tensor data: application to white matter fiber tract mapping in the human brain. Magn. Reson. Med. 42, 526–540.
Pistorio, A.L., Hendry, S.H., Wang, X., 2006. A modified technique for high-resolution staining of myelin. J. Neurosci. Methods 153, 135–146.
Tournier, J.D., Calamante, F., Gadian, D.G., Connelly, A., 2004. Direct estimation of the fibre orientation density function from diffusion-weighted MRI data using spherical deconvolution. NeuroImage 23, 1176–1185.
Tournier, J.D., Calamante, F., Connelly, A., 2007. Robust determination of the fibre orientation distribution in diffusion MRI: non-negativity constrained super-resolved spherical deconvolution. NeuroImage 35, 1459–1472.
Tournier, J.D., Yeh, C.H., Calamante, F., Cho, K.H., Connelly, A., Lin, C.P., 2008. Resolving crossing fibres using constrained spherical deconvolution: validation using diffusion-weighted imaging phantom data. NeuroImage 42, 617–625.
Tournier, J.D., Calamante, F., Connelly, A., 2010. Improved probabilistic streamlines tractography by 2nd order integration over fibre orientation distributions. Proc. 18th Annual Meeting of the Intl. Soc. Mag. Reson. Med. (ISMRM), p. 1670. Stockholm, Sweden, 2010; 18.
Wadghiri, Y.Z., Helpern, J.A., 2007. MR of transgenic mice. NMR Biomed. 20, 151–153.
Waerzeggers, Y., Monfared, P., Viel, T., Winkeler, A., Jacobs, A.H., 2010. Mouse models in neurological disorders: applications of non-invasive imaging. Biochim. Biophys. Acta 1802, 819–839.

Please cite this article as: Calamante, F., et al., Super-resolution track-density imaging studies of mouse brain: Comparison to histology, NeuroImage (2011), doi:10.1016/j.neuroimage.2011.07.014